New family of Type V eutectic solvents based on 1,10-phenanthroline and their application in metal extraction

Anna P.S. Crema, Nicolas Schaeffer, Henrique Bastos, Liliana P. Silva, Dinis O. Abranches, Helena Passos, Maria C. Hespanhol, João A.P. Coutinho

PII: S0304-386X(22)00156-6

DOI: https://doi.org/10.1016/j.hydromet.2022.105971

Reference: HYDROM 105971

To appear in: *Hydrometallurgy*

Received date: 2 May 2022

Revised date: 7 October 2022

Accepted date: 11 October 2022

Please cite this article as: A.P.S. Crema, N. Schaeffer, H. Bastos, et al., New family of Type V eutectic solvents based on 1,10-phenanthroline and their application in metal extraction, *Hydrometallurgy* (2022), https://doi.org/10.1016/j.hydromet.2022.105971

New family of Type V eutectic solvents based on 1,10-phenanthroline and their application in metal extraction

Anna P.S. Crema,[a,b] Nicolas Schaeffer,[a*] Henrique Bastos,[a] Liliana P. Silva,[a] Dinis O. Abranches,[a] Helena Passos,[a] Maria C. Hespanhol,[b] João A.P. Coutinho[a]

[a] CICECO - Aveiro Institute of Materials, Department of Chemistry, University of Aveiro, 3810-193 Aveiro, Portugal.

[b] Group of Analysis and Education for Sustainability (GAES), Chemistry Department, Federal University of Viçosa (UFV), Viçosa, MG 36570–900, Brazil.

* Corresponding email: nicolas.schaeffer@ua.pt

Abstract

Although a theoretically extensive number of hydrophobic eutectic mixtures suitable for solvent extraction are obtainable, to date reported mixtures rely on a limited number of chelating groups, namely phosphine oxide, carboxylic acid, and ketones. Herein, a new family of Type V Deep Eutectic Solvents (DES) based on the polypyridyl ligand 1,10-phenanthroline (phen) is presented with the aim of facilitating the extrapolation of the disclosed findings to other potential systems based on phen or bipyridine derivatives. The hydrophobic eutectic solvent composed of the natural phenolic extract thymol with phen exhibits a solid-liquid phase diagram with a useable liquidus compositional range on the thymol-rich side. The physical properties of the mixture are dependent on the presence of solutes liable to change the nature of the existing hydrogen-bonded network, most notably through the protonation of phen. The metal chelating ability of phen are retained when included as a DES component. Quantitative extraction of various transition metals cations (Cd(II), Mn(II), Co(II), Ni(II), Cu(II) and Zn(II)) as well as the platinum group metal Pd(II) was obtained across a range of solvent compositions. The extraction of Li(I), Mn(II), Co(II) and Ni(II) was further studied as a function of the aqueous phase pH, with the extent of metal partition decreasing with the protonation of phen at pH values below 1.0. Building upon the luminescent properties of phen, the eutectic solvent was further applied as a simultaneous pre-concentration and quantification medium for Fe(II/III), allowing for the facile UV-vis detection of Fe up to 12 μg L^{-1}.

Keywords: Deep eutectic solvent; Polypyridyl ligand; Solvent extraction; Luminescence; Metal detection.

Introduction

Polypyridyl ligands, of which 1,10-phenanthroline and 2,2′-bipyridine are the best-known base units, exhibit a high complexation affinity with many metal ions and represent versatile starting blocks for molecular recognition and supramolecular chemistry (Bencini and Lippolis, 2010; Hancock, 2013; Sammes and Yahioglu, 1994). The ligand 1,10-phenanthroline (thereafter referred to as phen) is a hydrophobic and electron-poor heteroaromatic bidentate ligand with the two nitrogen atoms forced in permanent juxtaposition due to its rigid planar structure. A further peculiarity of phen and its substituted derivates is the poor σ-donor ability of the heteroaromatic nitrogen atoms and their π-electron deficiency, making them excellent π acceptors (Anderegg, 1963a, 1963b). These structural features, namely its planarity, rigidity, hydrophobicity, and electron deficiency, determine the metal coordinating ability of phen and the resulting application of its chelates. For example, the planarity of phen allows its intercalation or groove binding with DNA or RNA whilst the $[Cu(phen)_2]^{2+}$ complex is commonly used as DNA marker and cleaving reagent (Meijler et al., 1997).

Phen presents a high complexation constant with d, and to a lesser extent f, block cations due to their stabilisation by favourable enthalpic contributions arising from the formation of strong coordination bonds with the nitrogen atoms (Anderegg, 1963a, 1963b; Hancock, 2013). Furthermore, the rigidity of phen and the permanent juxtaposition of the nitrogen donor atoms provides it an entropic advantage relative to its 2,2′-bipyridine analogue, resulting in enhanced kinetics of complex formation as well as increased surface activity at the oil-water interface due to its hydrogen bonding with water molecules (Burchett and Meloan, 1972; Lewis et al., 2011). The presence of low-energy π* orbitals gives rise to strong metal-to-ligand charge-transfer (MLCT) absorption bands with the aforementioned metals resulting in a range of luminescent phen compounds with emission bands spanning from the UV to the near infrared region (Accorsi et al., 2009). These properties can be further adjusted by the judicious grafting of substituents on the phen backbone and modification of the

aqueous phase composition, namely pH (pK_b(phen) = 4.86) (Accorsi et al., 2009; Bencini and Lippolis, 2010).

Increased organisation of phen derivatives and the covalent attachment of moieties to yield pincer-type ligands presenting size selective apertures were shown to increase the complexation constant and selectivity for a target cation (Carolan et al., 2012; Lewis et al., 2011; Tucker et al., 2020; Xu et al., 2016). An unexplored potential avenue to tune the extraction behaviour is by altering the energetic barrier to complexation through the inclusion of phen in pre-structured hydrogen-bonded assemblies. Type V deep eutectic solvents (DES) are binary mixtures of non-ionic compounds presenting an extreme eutaxia manifested as an important melting point depression relative to that predicted assuming thermodynamic ideality (Abranches et al., 2019). This non-ideal behaviour is assigned to the stronger intermolecular interactions between the DES components relative to those present in the pure precursors and is reflected in their solid-liquid equilibrium (SLE). Contrary to the dominant ionic interactions in Type I to IV DES (Smith et al., 2014), weak interactions, namely hydrogen bonding or other non-covalent interactions such as halogen bonding, dictate self-assembly in Type V DES (Abranches and Coutinho, 2022; Peloquin et al., 2021; Percevault et al., 2020; Schaeffer et al., 2021).

Type V DES incorporating at least one component with a chelating polar group and natural extract (terpenes, fatty acids, etc) show great promise for solvent extraction (SX) application as benign alternatives to conventional petroleum-derived diluents or ionic liquids. A range of desirable properties are obtainable through the appropriate selection of the hydrogen bond donor (HBD) and acceptor (HBA) including a wide liquidus composition, synergistic decrease in water solubility, moderate viscosities, and increased metal loading due to extractant concentrations of ≥ 50 mol% (Byrne et al., 2020; Gilmore et al., 2018; Schaeffer et al., 2020; Vargas et al., 2021). Furthermore, the varied energetic landscape provided by the extensive number of hydrogen bonded configurations in the DES phase accommodates the significant extraction of polar solutes and suppresses the third-phase formation that hinders traditional SX at higher metal loadings (Vargas et al., 2021). Type V DES were successfully applied to the extraction of transition metals (Schaeffer et al., 2020, 2018), Pd(II) and Pt(IV) (Vargas et al., 2021), U(IV) (Gilmore et al., 2018), As(III) (Rajput et al., 2021), In(III) (Edgecomb et al., 2020), Li(I) (Hanada and Goto, 2021), and Sm(III) (Ni et al., 2021). Importantly for their application, Vargas et al. (2021) demonstrated that metal extraction in Type V DES presents a non-linear behaviour dependent on the extractant molar fraction and

the extent of the thermodynamic deviation ideality. As such, extraction in a given DES must be rationalised with regards to its phase diagram.

Although a theoretically extensive number of Type V DES are obtainable through variations in HBD and HBA selection, reported mixtures for SX rely on a limited number of chelating groups, namely phosphine oxide, carboxylic acid, and ketones. Whilst the solid-liquid phase diagram of phenol and pyridine was reported over a century ago (Bramley, 1916), to the best of our knowledge no DES with polypyridyl ligands were reported despite the numerous relevant properties of their complexes. The incorporation of these chelating agent paves the way for a new family of Type V DES and the development of functional fluids with industrially relevant properties, from the SX of metal ion for analytical pre-concentration to luminescent materials. In this work, the DES composed of phen with the prototypical HBD thymol is introduced and its relevant physical-chemical properties characterised (Abranches et al., 2019). Its use in SX for a range of metal ions is presented and the extraction mechanism elucidated. Additionally, the luminescent properties of the loaded DES phases after extraction are briefly addressed. The results herein provide a framework for the development of new and versatile class of Type V DES.

Methodology

Materials and Instrumentation

The DES constituents, dehydrated 1,10-phenanthroline (≥ 99 wt.%), chlorothymol (99 wt.%) and 2,6-di-tert-butyl-4-methylphenol (BHT, 99 wt.%), were obtained from Sigma-Aldrich (USA) and thymol (99 wt.%) from TCI (Japan). The metal salts cobalt chloride hexahydrate (99 wt.%), lithium chloride monhydrate (99 wt.%), manganese chloride tetrahydrate (99 wt.%), iron chloride hexahydrate (99 wt.%), zinc chloride (98 wt.%) were obtained from Merck (USA); nickel chloride hexahydrate (99 wt.%), cadmium bromide tetrahydrate (98 wt.%) and barium chloride dihydrate (99 wt.%) were purchased from BDH Chemicals (UK), lanthanum chloride heptahydrate (99 wt.%) from Fluka (VWR, USA) and palladium chloride (99 wt.%) from Sigma-Aldrich. Hydrochloric acid (37 wt.%) was purchased from Fisher Scientific (USA). Solutions were prepared using UP ultrapure water, double distilled, passed through a reverse osmosis system and then treated with a Milli-Q (USA) water purification device (18.2 mΩ at 298 K) was used for all the experiments.

All systems were gravimetrically prepared through careful weighing of each component using an analytic balance Mettler Toledo XP205 (USA; uncertainty 0.0001 g). Proton nuclear magnetic resonance (^{1}H-NMR) analysis was performed using a Bruker Avance 300 (USA), operating at 75 MHz. Deuterated water with tetramethylsilane as the reference was added to the sample in a co-axial insert. Raman spectra were acquired on a Bruker MultiRAM (USA) equipped with a 1064 nm Nd-YAG laser source and a nitrogen cooled germanium detector. All spectra were recorded in the 3600 to 100 cm^{-1} range with a resolution of 4 cm^{-1} (laser power of 100 mW and 400 scans) and deconvoluted into Gaussian components using the Origin software package. Fluorescence analysis of the loaded DES phase following extraction of Co(II), Ni(II) or Mn(II) was performed using a Jasco FP – 8300 fluorimeter (USA) under emission mode (excitation band of 425 nm) in the spectral range 435 – 750 nm, scan 200 nm min^{-1}. Samples were diluted in acetonitrile except for manganese samples, which were diluted in methanol due to the appearance of a precipitate. Powder X-ray diffraction (P-XRD) was determined using a Malvern Panalytical Empyrean (UK) with Cu Kα radiation operating with a Cu anode ($K_{\alpha1}$= 1.5406 Å; $K_{\alpha2}$= 1.5444 Å) at 45 kV and a spinning discs sample holder. Diffractograms were analysed using the X'pert Highscore Plus software package and the patterns matched against those in the International Centre for Diffraction Data (ICDD) database.

Metal quantification was performed using a Picofox S2 (Bruker Nano, USA) total reflection X-ray fluorescence spectrometer (TXRF) with a molybdenum X-ray source. The voltage of the X-ray tube was 50 kV and the current 600 µA. All carriers were first treated with 10 µL of silicon in isopropanol solution and dried at 353 K for 30 min. Aqueous phase samples were diluted in 0.5 wt.% polyvinyl alcohol acidified at pH = 2.0 using HCl and spiked with a known concentration of YCl_3 (1000 ppm Certipur® standard, Sigma-Aldrich) to obtain a final standard element concentration of 1 to 10 ppm (mg L^{-1}) depending on the sample metal content. Ten microliters of each solution containing the metals and yttrium standard were added onto a treated carrier and dried on a hot plate at 353 K for 30 min. The acquisition time was varied from 120 to 1000 seconds in function of the sample concentration. Lithium was quantified after dilution using an ion-selective electrode (Mettler Toledo Dx-series, USA) using a LiCl calibration curve from 0.1 to 10.0 mmol L^{-1}. Magnesium sulfate was used to maintain a constant ionic strength.

Determination of phase diagrams and SLE modeling

Binary mixtures of phen with a HBD (thymol, chlorothymol or BHT) were prepared in different proportions covering the full composition range (at 0.1 mole fraction intervals) using an analytic balance Mettler Toledo XP205 under ambient conditions. Samples were heated under stirring at 353 K until a homogenous liquid was obtained and then stirred for an additional 30 min. Samples were left to crystallise at room temperature. Two experimental methods were applied to determine the melting temperatures depending on the physical state of the resulting mixture. For fully re-crystallised mixtures, samples were ground and packed into a glass capillary and the melting temperature measured using an automatic glass capillary device model M-565 from Buchi (Switzerland) with a temperature resolution of 0.1 K min^{-1}. For mixtures presenting a pasty texture (partial re-crystallisation), these were gradually heated until complete melting and the temperature was controlled with a PT100 probe with a precision of ±0.1 K. The probe was previously calibrated against a certified platinum resistance thermometer, SPRT100 (Fluke-Hart Scientific 1529 Chub-E4), traceable to the National Institute of Standards and Technology (NIST). Each procedure was repeated at least three times with the average result reported.

The SLE of the eutectic mixtures with complete immiscibility in the solid phase can be described by equation (1) (Prausnitz et al., 1999):

$$\ln\left(x_i\gamma_i^l\right) = \frac{\Delta_m H_i}{R}\left(\frac{1}{T_{m,i}} - \frac{1}{T}\right) + \frac{\Delta_m Cp_i}{R}\left[\frac{T_{m,i}}{T} - ln\left(\frac{T_{m,i}}{T}\right) - 1\right] \quad \text{-(1)}$$

where x_i is the mole fraction of component i and γ_i^l its activity coefficient in the liquid phase, T is the absolute temperature, R is the ideal gas constant, $T_{m,i}$, $\Delta_m H_i$ and $\Delta_m Cp_i$ are the melting temperature, enthalpy and heat capacity change of the pure solute, respectively. When the differences between the eutectic and the melting temperatures of the pure compounds are small (< 100 K), as is the case in the studied systems (see **Figure 1**), the term related with heat capacities may be neglected due to its small contribution to the phase equilibrium calculations (Coutinho et al., 1995), yielding Equation (2):

$$\ln\left(x_i\gamma_i^l\right) = \frac{\Delta_m H_i}{R}\left(\frac{1}{T_{m,i}} - \frac{1}{T}\right) \quad \text{-(2)}$$

When ideality is assumed, γ_i^l equals to 1 and the solubility curves are derived from Equation (2). The experimental activity coefficients are obtained through Equation (2) using the experimental temperature data.

Characterisation of thymol+phen eutectic

The stability and properties of the thymol+phen eutectic system for a phen molar fraction of x_{Phen} = 0.2 was assessed as a function of the aqueous phase composition after contacting the eutectic phase with an aqueous phase of varying acidity from 0.0 to 1.0 mol L^{-1} of HCl in the absence of metal ions. The samples were left to equilibrate for 2 h at 298 K and an organic to aqueous phase ratio (O:A) of 0.5 prior to centrifugation at 10,000 rpm for 10 min and isolation of the DES phase. The water content of the DES phase was determined by Karl Fischer (KF) titration using a Titroline 7500 KF Trace (Metrohm, Switzerland) whilst the acid concentration was determined by acid-base titration before and after contacting using phenolphthalein as an indicator. The loss of phen from the DES to the aqueous phase was measured by UV-vis on a Shimadzu UV-1800 spectrophotometer (Japan), with the obtained calibration shown in **Figure S1**. Analyses were performed in triplicate with the average result reported. Viscosity was determined using a viscometer-densimeter SVM 3000 Anton Paar Rotary Stabinger (Austria), with a temperature uncertainty of ± 0.1 K and a relative uncertainty of dynamic viscosity of ± 0.35 %. A thermostatic bath (ME-18 V Visco-Thermostat, Julabo, (Germany) ± 0.1 K) was used for temperature control.

Metal extraction in the thymol+phen eutectic

Metal ion extraction in the thymol+phen eutectic was assessed as a function of the aqueous phase acid concentration (0.0 to 3.0 mol L^{-1}), counter anion selection (chloride, nitrate, sulphate), eutectic mol fraction (x_{Phen} = 0.2-0.3) and metal to phen ratio. Unless otherwise specified, standard conditions were metal concentrations of 0.02 mol L^{-1}, [HCl] = 0.05 mol L^{-1}, a phen molar fraction 0.2 and an organic to aqueous phase ratio of 0.50 (total volume of 1.5 mL). The systems were mixed under constant agitation of 1000 rpm for 1 min using an Eppendorf Thermomixer Comfort equipment (Germany) and thereafter left to rest for 45 min at room temperature. The systems were centrifuged for 10 min and rotated at 10,000 rpm and the phase separated with the aqueous phase analyzed by TXRF and ion-selective electrode potentiometer following appropriate dilution. All analyses were performed in triplicates with the average result reported. Metal ion (M^{n+}) distribution coefficients (D_M), extraction efficiencies (%EE_M), and the separation factor between two given metals ($\alpha_{M1/M2}$) are calculated using Equations (3) to (5) respectively:

$$D_M = \frac{[M]_{DES,f}}{[M]_{aq,f}} \quad \text{-(3)}$$

$$\%EE_M = \frac{([M]_{aq,ini} - [M]_{aq,f})}{[M]_{aq,ini}} \times 100 \quad \text{-(4)}$$

$$\alpha_{M_1/M_2} = \frac{D_{M1}}{D_{M2}} \quad \text{-(5)}$$

where the subscripts ini and f indicate the sampling timeframe before (ini) or after (f) extraction whilst DES and aq indicate the DES and aqueous phase, respectively. The DES phases after extraction of Co(II), Ni(II) or Mn(II) were further analyzed by fluorescence analysis following phase separation.

The detection limit of thymol+phen DES (x_{Phen} = 0.2) for $FeCl_3$ was performed by UV-vis analysis of the DES phase. Briefly, 0.25 mL of DES were agitated for 1 min with various aqueous $FeCl_3$ solutions at pH = 5.5 and O/A = 0.25 (total volume 1.25 mL) and centrifuged thereafter. The DES phase was analysed by UV-vis using a Synergy HT microplate reader from Biotek Instruments (USA). The DES phase volume per sample well was 0.15 mL.

Simulation

Molecular dynamic (MD) simulations of the thymol+phen system for x_{phen} = 0.2 (400 molecules of thymol and 100 molecules of phen) in the presence of water and HCl were carried out using Gromacs 5.1 package (Abraham et al., 2015) within the NpT ensemble by adopting the leapfrog algorithm to integrate the equations of motion at a fixed temperature (298 K) and pressure (1 bar) (Hockney et al., 1974). The non-polarizable OPLS all atom force field was used for phen and thymol, the optimised OPLS-AA forcefield was used for H_3O^+ and Cl^-(Bonthuis et al., 2016) and water molecules were represented by the SPC/E model (Berendsen et al., 1987). Phen and thymol partial charges were refined by DFT calculations using Gaussian09 (Frisch et al., 2009) employing Becke's three-parameter exchange (Becke, 1988) in combination with the Lee, Yang, and Parr correlation functional (Lee et al., 1988) at the B3LYP/6−311+G(d,p) level of theory. Atomistic charges were determined using the CHELPG methodology and applied with no charge scaling factor (Breneman and Wiberg, 1990). Hydrogen bonds were constrained by the LINCS algorithm (Hess et al., 1997) whilst LJ and Coulombic interactions were computed up to a cut-off radius of 1.2 nm. Long-range Coulombic interactions were evaluated by particle mesh Ewald (PME) (Darden et al., 1993). The temperature and pressure were controlled through the Nose–Hoover thermostat (Evans and Holian, 1985) and the Parrinello–Rahman barostat (Parrinello and Rahman, 1981), respectively. All simulations were started from a randomly distributed configuration and production runs were carried for 100 ns. The MD simulation outputs were visualized using the VMD software package (Humphrey et al., 1996). Domain analysis was

obtained using the TRAVIS post-processing package (Brehm et al., 2015a; Brehm and Kirchner, 2011).

The Conductor like Screening Model for Real Solvents (COSMO-RS) is a statistical thermodynamics model that predicts the chemical potential (and activity coefficients) of individual components in liquid mixtures (Eckert and Klamt, 2002; Klamt, 1995; Klamt et al., 1998). To do so, it relies on pair-wise interactions between screened charge surface patches of each molecule (the so-called σ-surface), obtained using DFT and the COSMO continuum solvation model. Given its ability to predict activity coefficients, COSMO-RS can be coupled with Equation 2 to estimate SLE phase diagrams. This was explored in this work to predict the SLE phase diagrams of thymol+2,2'-bipyridine. The necessary σ-surfaces were obtained using the COSMO-BP-TZVP template of the software package TURBOMOLE (TURBOMOLE V7.1 2016), which utilizes the def-TZVP basis set, the BP-86 DFT functional, and the COSMO solvation model with ideal screening (infinite permittivity). All COSMO-RS calculations were performed in the software package COSMOtherm (BIOVIA COSMOtherm, 2021) using the BP_TZVP_21 parametrization.

Results and Discussion

Phase diagram

Considering the breadth of phen-based DES applications that can be modulated through rational HBD selection, the following discussion summarizes the HBD influence on the HBD+phen phase diagram thereby providing a guideline for the design of phen-based Type V DES. The presence of hydrogen bonding in-itself is not a guarantee of "deep" eutectic solvent formation especially if the individual components already establish hydrogen bonds in their pure state. Whilst the ΔpK_a difference between the hydrogen bond donor and acceptor couple provides an initial estimation of the hydrogen bond strength (Gilli et al., 2009), components presenting an important degree of self-association (e.g. carboxylic acid dimers) tend to yield ideal mixtures as was reported for alcohol+carboxylic acid systems ($\Delta pK_a > 10$) (Martins et al., 2018). The addition of electron-withdrawing groups by resonance effect in the case of phenolic compounds (Abranches et al., 2019) or by halogenation (hydrogenated *vs* fluorinated alcohols) (Isabel Cabaço et al., 2021) minimises self-association by increasing the acidity of the HBD group whilst reducing the basicity of the HBA. A final consideration is

the concept of "anti-crystal engineering" design rule when selecting HBA/HBD combinations to promote low melting temperatures and avoid the formation of co-crystals (Dean et al., 2009). This is relevant in the case of phen-based systems as its lack of configurational entropy imposed by its symmetry and rigidity makes the formation of co-crystal likely due to the directionality of the resulting HBA-HBD pair.

To illustrate these principles, the solid-liquid phase diagrams of phen with three phenolic compounds as HBD, namely thymol, chlorothymol or 2,6-di-tert-butyl-4-methylphenol (BHT) as HBD (structures shown in **Figure 1A**), were determined and presented in **Figure 1B**. The SLE data and derived activity coefficients are available in **Table S1** and **Figure S2** of the ESI, respectively, whilst the melting properties used to calculate the ideal solid-liquid phase diagrams (dashed lines) are available in **Table S2**. Importantly, anhydrous phen was used in this study; phen is often available in its monohydrated form and the presence of water is known to induce strong changes on the SLE (Abranches et al., 2021). Although the systems were prepared under ambient conditions, care was taken to minimise water exposure and the maximum water content of the prepared systems never exceeded 0.32 wt.% H_2O.

Thymol, in addition to being a natural extract, was previously identified as an excellent HBD in systems with alcohols (Abranches et al., 2019) or phosphine oxide (Schaeffer et al., 2020) and serves as the starting point of this study. For comparative purposes, the reported SLE diagram of phenol+pyridine is shown in **Figure 1C** (Bramley, 1916). The thymol+phen system is characterised by two eutectic points at approximately x_{phen} ~ 0.3 and 0.5, similarly to that in the phenol+pyridine system. A quasi-ideal behavior is observed on the phen-rich side of the phase diagram whilst important negative deviations from ideal behavior on the thymol-rich side ($\gamma < 0.5$, **Figure S2**) yields a useable liquidus range of x_{phen} = 0.2 to 0.3 at 298 K. The XRD of the thymol+phen eutectic for x_{phen} = 0.5 in **Figure S3** shows the emergence of additional peaks relative to that of the starting components or x_{phen} = 0.9, suggesting the presence of a different solid phase at that composition.

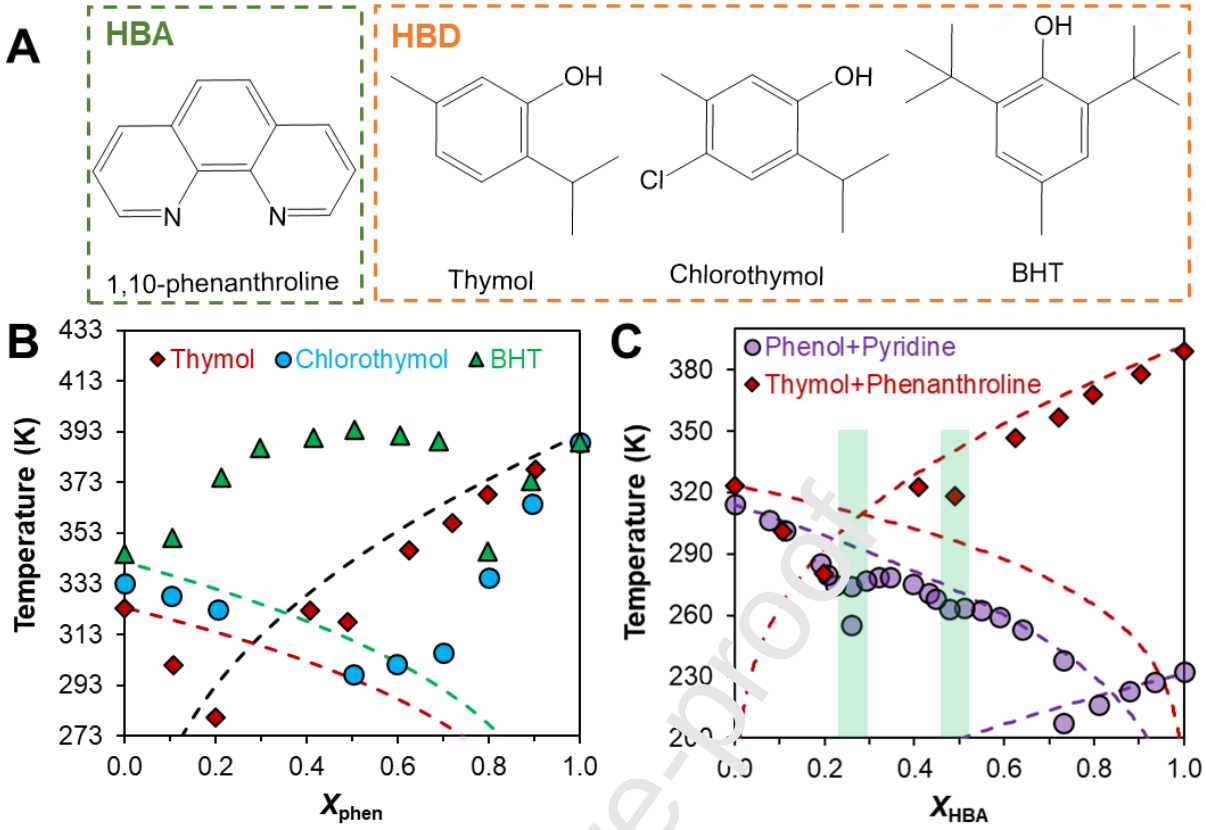

Figure 1. A) Structures and B) Experimental solid-liquid phase diagram of 1,10-phenanthroline with thymol, chlorothymol and 2,6-di-tert-butyl-4-methylphenol (BHT). C) Comparison of the phase diagrams of thymol+phen with phenol+pyridine (adapted from (Bramley, 1916)) with the overlapping eutectic transitions highlighted. Dashed lines represent the ideal solid-liquid phase diagrams.

Substitution of the para hydrogen of thymol by the electron-withdrawing chloride in chlorothymol results in a markedly different SLE diagram (**Figure 1B**) with an increased liquidus compositional range from x_{phen} = 0.3 to 0.5 at 298 K and the likely existence of a peritectic around x_{phen} = 0.7. Contrary to the thymol+phen system, the chlorothymol+phen system presents a maximal negative deviation from ideality on the phen-rich side for x_{phen} = 0.7 (**Figure S2**) resulting in a melting point depression of over 40 K at that composition. Finally, the SLE of the BHT+phen system is defined by a eutectic point at x_{phen} = 0.8 and the clear formation of a co-crystal with a 1:1 stoichiometry confirmed by XRD analysis (**Figure S4**). This is to be expected due to the steric constraints imposed by the two tert-butyl groups of BHT positioned either side of the phenolic proton and forcing a 1:1 perpendicular interlocking arrangement of BHT with phen. The analysis of the systems in **Figure 1B** is

simplified by the lone HBA nature of phen and the permanent juxtaposition of its nitrogen atoms. Although not experimentally studied within this work, COSMO-RS simulation suggests that replacement of phen with the more configurationally flexible 2,2'-bipyridine presents a more complex SLE that depends on the equilibrium of the trans and cis isomer in the eutectic at a given composition as shown in **Figure S5**. As such, care must be taken when transposing phen-based solid-liquid diagrams to the equivalent 2,2'-bipyridine systems.

Characterisation of the thymol+phen system – viscosity and density

In the following sections, the discussion focuses on the thymol+phen system at the molar fraction x_{phen} = 0.2 with the system characterization revolving around the relevant properties for SX application, namely viscosity, density, chemical stability and co-extraction of water and acid. The composition of x_{phen} = 0.2 was chosen as compromise between expected performance ([phen] = 1.28 mol kg^{-1}) and toxicity of the DES, with phen presenting a LD50 (oral, rat) of 132 mg kg^{-1} compared to 980 mg kg^{-1} for thymol (SigmaAldrich, 2022). Three different systems were studied to understand the evolution of the viscosity and density profiles in the DES phase as a function of the aqueous phase composition in SX: (i) the "dry" DES after preparation and after equilibration with (ii) water or (iii) 1.0 mol L^{-1} HCl. These are presented in **Figure 2** as a function of temperature from 293.15 to 323.15 K and summarized in **Table S3-S4**. The viscosity (η) was fitted with the Arrhenius equation (Equation 6) whilst a linear fit was employed to fit the density data. The fit parameters are summarised in **Table S5**.

$$\eta = Ae^{\left(\frac{E_A}{RT}\right)} \quad \text{-(6)}$$

where A is the pre-exponential factor (Pa s), E_A the activation energy (J mol^{-1}), R is the universal gas constant (J mol^{-1} K^{-1}) and T is the temperature (K). Whilst the fit of the viscosity data was satisfactory at the studied conditions (R^2 > 0.99), it is likely that the Vogel–Tamman–Fulcher equation would provide a better estimation for temperatures nearing the solid-liquid transition as the system non-ideality becomes more pronounced.

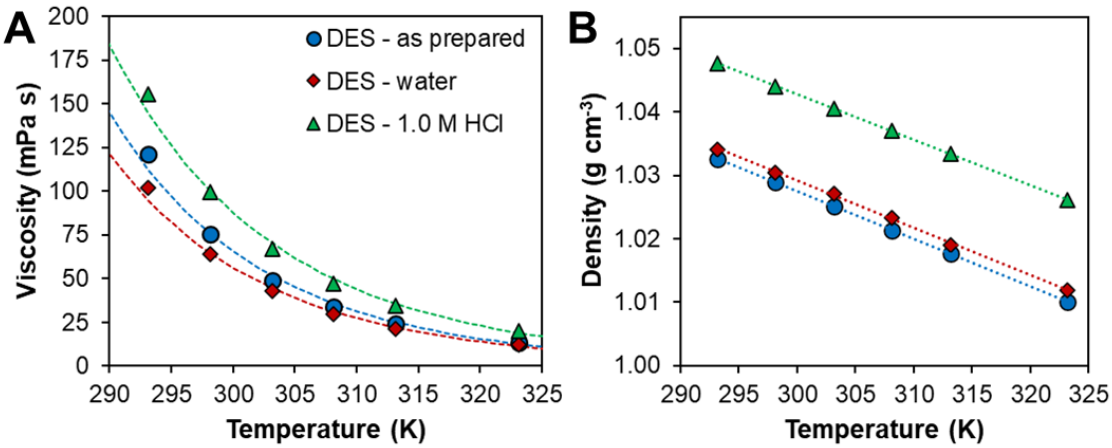

Figure 2. A) Viscosity and B) density of the thymol+phen eutectic (x_{phen} = 0.2) after preparation ([H_2O] = 0.28 ± 0.01 wt.%), and after equilibration with water ([H_2O] = 1.63 ± 0.04 wt.%) or 1.0 mol L^{-1} HCl ([H_2O] = 1.85 ± 0.14 wt.%; [HCl] = 0.65 ± 0.02 wt.%). Fitted line parameters are available in **Table S5**.

Viscosity provides a macroscopic indication to the strength and extent of the intermolecular hydrogen bond network in DES. At 298.15 K, the thymol+phen DES has a viscosity of 75.31 mPa s, comparable to that in the strongly non-ideal thymol+trioctylphosphine oxide (x_{thymol} = 0.5, η = 69.93 mPa s)(Schaeffer et al., 2020) but more than for quasi-ideal mixtures such as thymol+decanoic acid (x_{thymol} = 0.5, η = 12.16 mPa.s)(Martins et al., 2018). Water saturation of the DES decreases the viscosity to 63.94 mPa s whilst equilibration with a 1.0 mol L^{-1} HCl solution increases it to 99.63 mPa s. As will be discussed below, these changes are assigned to the (i) weakening of the HBD-HBA interaction upon inclusion of water and (ii) increased re-structuration of the DES phase to accommodate the presence of ionic solutes coming from the acid (H^+ and Cl^-) and protonated phen ($[phenH]^+$). In all cases, the activation energies (E_A) exceed 50.0 kJ mol^{-1} with the pure DES exhibiting the highest E_A = 57.1 kJ mol^{-1} (**Table S5**) and is consistent with that of viscous fluids. Problematically for its application in SX, densities of the tested DES systems are close to that of water making phase de-mixing difficult in the absence of centrifugation. The concentration of polar solute in the DES phase increases its density, resulting in an aqueous/organic phase inversion upon metal extraction in 1.0 mol L^{-1} HCl (*vide infra*).

Characterisation of the thymol+phen system – pH dependency and structure relationship

In aqueous media, phen acts as a weak base with a pK_b of 4.86 and presents pH-dependent properties which can translate into diminished metal complexation (Accorsi et al., 2009). Furthermore, formation of the [phenH]Cl salt will have strong repercussions on the properties of the DES as the melting point of [phenH]Cl monohydrate is of approximately 497 K, far above that of neutral phen (Honeywell Research Chemicals, 2022). However, protonation constants are known to vary by several orders of magnitude in organic media (Sarmini and Kenndler, 1999) making the translation of pK_b from the aqueous to the DES phase impossible. Although the pK_b of phen-derivatives is often determined by titration using UV-vis, the important phen concentration and molar attenuation coefficient poses a practical problem as excessive dilution breaks the defining structure of DES into its simple solvated components (Hammond et al., 2017). As such, the protonation of phen in the thymol+phen eutectic was followed by ^{1}H-NMR by equilibrating the DES phase with aqueous solutions of varying acidity from 0.0 to 1.0 mol L^{-1} (pH = 0.0) at an O:A = 0.50. By placing the deuterated solvent as a co-axial insert, the DES phase was not diluted for analysis. The resulting spectra, focusing on the aromatic and hydroxyl protons, are presented in **Figure 3**. Complimentarily, the extracted water and acid content to the DES phase was determined for each system and are reported in **Table S5**.

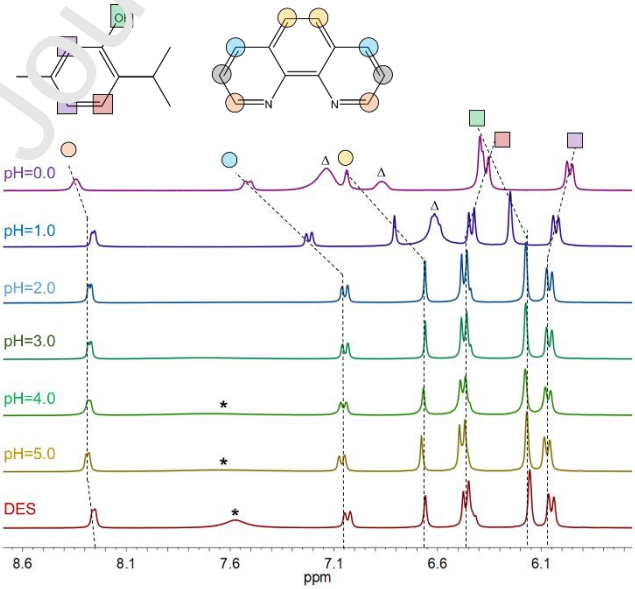

Figure 3. ^{1}H-NMR analysis of the initial aqueous phase acidity influence on the thymol+phen eutectic phase (x_{phen} = 0.2; O:A = 0.50). Stars and triangles represent unassigned peaks that do not appear in all spectra.

Acidification of the aqueous phase has little influence on the DES phase structure for pH > 1 ([HCl] < 0.1 mol L^{-1}). Further addition of HCl results in an upshift of the phen protons as well as the hydroxyl proton of thymol, reflecting their less shielded environment. The opposite is observed for the aromatic protons of thymol. The asymmetry in the phen and thymol shifts is indicative of the restructuration of the DES phase into more explicitly segregated polar and apolar nano-domains. The onset of the ^{1}H-NMR shift correlates well with the increased HCl extraction to the DES phase as shown in **Figure S6** and suggests that the change in the DES self-organization is acid-driven as the water content is approximately constant for pH > 1 (**Table S6**). For an initial aqueous phase HCl concentration of 1.0 mol L^{-1}, a final HCl content in the DES phase of 0.18 mol kg^{-1} was obtained, representing a H^{+} to phen ratio of ~0.14. Furthermore, the protonation of phen could be visually followed as the DES phase took on a strong yellow color when in contact with 1.0 mol L^{-1} of HCl consistent with the red-shifted spectra of $[phenH]^{+}$ relative to phen (Armaroli et al., 1992). Overall, it appears that partial protonation of phenanthroline in DES occurs for an aqueous phase pH of ≤ 1.0, almost four orders of magnitude lower than for the pure compound in water. A series of shift in **Figure 3** identified by the triangle symbols do not appear in all spectra and likely reflect some broad π - π interactions and/or resonance effects upon protonation of phen.

The favorable free energy of complexation driving ion partition in SX is quenched by the energetic penalty from (i) solvent nanostructure reorganization around the extracted and co-extracted species, (ii) the confinement of ionic solutes in small polar volumes and (iii) excess free energy of the water/ion mixture (Bourgeois et al., 2020). Considering the non-ideality of DES stemming from their pre-organised hydrogen bonded structure, any significant changes to the latter from the partition of acid and water is liable to affect the extraction mechanism. In fact, Pd(II) extraction in the thymol+trioctylphosphine oxide was shown to occur only upon HCl co-extraction and the breaking of the DES hydrogen bonded-network (Vargas et al., 2021). As such, the concentration of extracted water and acid to the DES phase in **Table S6** was converted to molar percentage to better follow the change in the DES composition with the results shown in **Figure 4A**. To simplify the calculations, it was assumed that no

significant transfer of the DES component to the aqueous phase takes place. As will be shown later, this assumption holds only for aqueous phase pH values above the protonation of phen, below this pH the partition of [phenH]Cl to the aqueous phase occurs. In agreement with the ^{1}H-NMR results in **Figure 3**, the DES composition is unchanged until [HCl] ≥ 0.1 mol L^{-1} after which a non-negligible amount of acid and water are co-extracted. These extracted polar solutes make up one third in mol.% of the final DES phase in equilibrium with an aqueous phase of [HCl] = 3.0 mol L^{-1}, yielding a final H^{+} to phen ratio of 0.31.

To further probe the influence of these polar solutes on the DES structure, four MD simulations of the thymol+phen system at fixed ratio of 4:1 were carried out with increasing polar solute concentrations mirroring the experimental compositions, namely (1) pure DES, (2) x_{H2O} = 0.12, (3) x_{H2O} = 0.17 and (4) x_{H2O} = 0.16 with x_{HCl} = 0.02 (simulated as the dissociated Cl^{-} and H_3O^{+} ions). The nano-structuring of the DES phase was estimated by calculating the number of polar domains and the volume of the largest domain based on the Voronoi tessellation method (Brehm et al., 2015b). The polar domains are defined as the subset composed of H_2O, H_3O^{+} and Cl^{-} molecules, the nitrogen atoms of phen and hydroxyl group of thymol, with the results presented in **Figure 4B**. A domain number greater than 1 is indicative of a dispersed subset. Additionally, representative snapshots of the equilibrated simulations with increasing polar solute fraction are provided in **Figure 4C** to illustrate the discussion. Addition of polar components in the DES phase results in the reduction in the number of discrete molecular-scale domains as these coalesce into larger assemblies as shown by the important polar domain volumes. Interestingly, a small addition of HCl did not change the domain number for a constant x_{H2O} but yielded an increase in the maximum volume which is expectable upon the introduction of electrostatic interactions to a non-ionic system. Overall, the observed behaviour in **Figure 4** parallels the hierarchical self-assembly observed in the organic phase of conventional SX systems, albeit without third-phase formation (Clark, 2019; Motokawa et al., 2019).

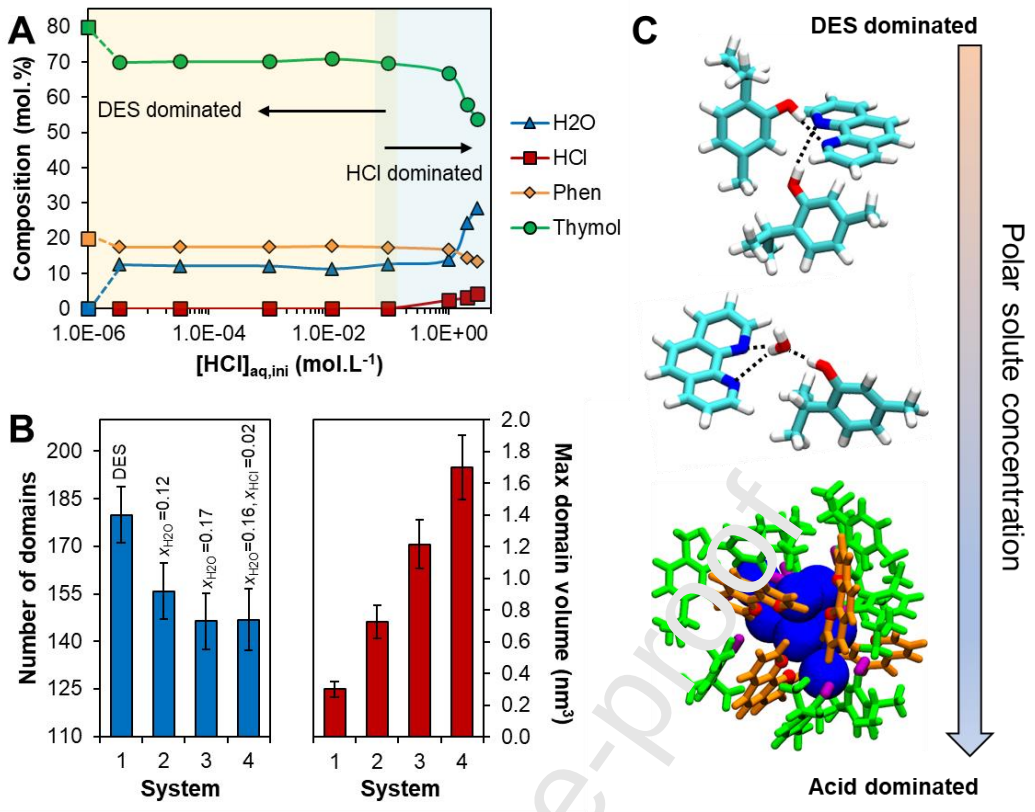

Figure 4. A) Influence of the initial aqueous phase HCl concentration on the thymol+phen eutectic phase composition at equilibrium (x_{phen} = 0.2; O:A = 0.50). The extracted water and acid content to the DES phase was determined for each system and are reported in **Table S6**. Square symbols represent the composition in the pure DES. B) MD-derived number of polar domains and volume of the largest continuous one in the DES phase as a function of the H_2O and HCl molar fraction in the system. C) Representative examples of the change in the dominant aggregate obtained from MD simulations upon increased concentration of polar solutes.

Co(II), Ni(II), and Mn(II) extraction in the thymol+phen system

Following its characterization, the potential of the thymol+phen eutectic for the SX of metal cations is now addressed. The extraction behaviour of Mn(II), Co(II), Ni(II) and Li(I) from multi-elemental solutions was followed in detail as a function of the HCl concentration in **Figure 5A**. These metals were selected due to their importance in achieving a green energy future and their forecasted demand in various associated applications including lithium ion batteries for energy storage (Herrington, 2021). Additionally, the influence of x_{phen} molar

fraction and the metal to the phen ratio was assessed (in the absence of Li(I)), with the results being presented in **Figure 5B-C**. All %EE and D values are available in **Table S7** to **S10**.

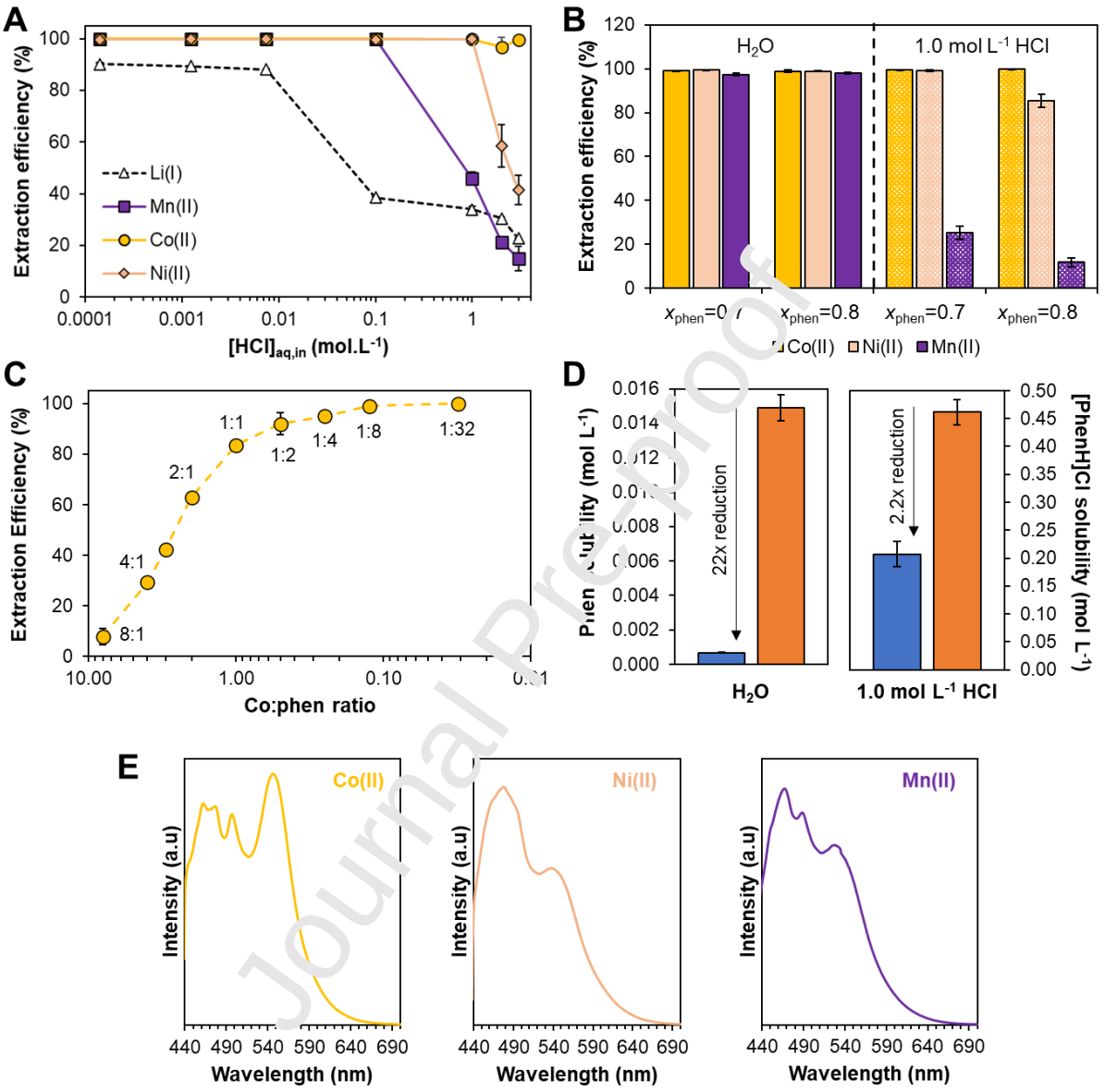

Figure 5. Extraction of Mn(II), Co(II) and Ni(II) in the thymol+phen eutectic as a function of the HCl concentration in the presence of [Li(I)] = 0.08 mol L^{-1}. Influence of B) x_{phen} molar fraction and C) Co(II) to phen ratio on the extraction. Standard conditions of [M] = 0.02 mol L^{-1}, pH = 5.5, x_{phen} = 0.2 and O/A = 0.5 were applied unless specified otherwise. D) Aqueous phase concentration of phen after equilibration of thymol+phen eutectic (x_{phen} = 0.2 and O/A = 0.5) with an aqueous phase of varying acidity, shown in blue. For comparison, the aqueous solubility of pure phen and [phenH]Cl were taken from (Burgess and Haines, 2002) and (Honeywell Research Chemicals, 2022) respectively and are shown in orange. E)

Fluorescence of the metal saturated thymol+phen eutectic after extraction of Co(II), Ni(II) an Mn(II) (x_{phen} = 0.2; O/A = 0.50, n(M(II)/n(phen) = 2) under emission mode (excitation band of 425 nm). Systems were diluted after extraction in acetonitrile except for Mn(II) where methanol was used.

Extraction results in **Figure 5A-B** indicate that Co(II) is quantitatively extracted across all tested aqueous phase and DES phase compositions. Incorporation of phen into the DES structure does not appear to penalize Co(II) extraction due to the favorable metal chelate formation. Up to 83.5% of Co(II) is extracted in the system containing an equimolar amount of metal to phen ([phen] = 1.28 mol kg^{-1}, pH = 5.5), as shown in **Figure 5C**, and plateaus thereafter for excess phen to metal ratios. As such, Co(II) can be extracted as $[Co(phen)_n]^{2+}$ (n=1-3) as function of the Co(II):phen ratio and allows for the intensification of SX by targeting concentrated leachate solutions using small organic phase volumes. Importantly, the final Co(II) concentration in the DES phase of 1.06 mol kg^{-1} causes it to solidify at room temperature following extraction and places a practical upper limit to the maximum loading concentration.

Contrary to Co(II) which presents a pH independent extraction, Mn(II) extraction drops sharply for aqueous phase HCl concentrations greater than 0.1 mol L^{-1} both in the presence or absence of Li(I). The decrease in Mn(II) extraction coincides with the onset of phen protonation, resulting in a α(Co/Mn) of 1975 for [HCl] = 1.0 mol L^{-1} (D_{Co} = 589, D_{Mn} = 0.30) in the absence of Li(I) (**Figure 5B**). To a lesser extent a decrease in Ni(II) extraction is also observed for aqueous phase HCl concentrations greater than 1.0 mol L^{-1}. Nevertheless, the increased selectivity towards Co(II) under acidic conditions occurs at the expense of [phenH]Cl loss to the aqueous phase as reported in **Figure 5D**. In spite of the large concentration in the DES phase, the solubility of phen in the aqueous phase at pH = 5.5 and O/A = 0.50 is 22 times lower than that of the pure component in water (Burgess and Haines, 2002), confirming the synergistic enhancement in hydrophobicity upon inclusion in a DES. The greater solubility of the derived salt [phenH]Cl means that approximately one-third of the phen content was lost to the aqueous phase upon contacting with 1.0 mol L^{-1} HCl at the same O/A ratio. As such, a compromise is required between metal extraction, selectivity, and integrity of the DES phase. Finally, neither the x_{phen} (**Figure 5B**) nor the salt counter-anion

(**Figure S7**) significantly influence the extraction efficiencies under the tested conditions, with a small rise in partition observed as the x_{phen} is increased.

Unexpectedly given that log(K_1) decreases from Ni(II) > Co(II) > Mn(II) (Hancock, 2013), extraction results indicate a preferential extraction of Co(II) > Ni(II) > Mn(II). To better understand the unexpected behaviour, Raman analysis of the loaded DES phase was performed for the individual transition metals ([M(II)] = 0.10 mol L^{-1}) at pH = 5.5 and is presented in **Figure S8**. The analysis focuses on the ring deformation vibrations of phen in the 700 to 740 region cm^{-1} which were shown to be sensitive to the interaction with transition metals (Muniz-Miranda et al., 2010; Thornton and Watkins, 1991). The Raman bands observed at 711 cm^{-1} (green) and 740 cm^{-1} (orange) do not shift compared to the DES phase with no metal, but there is a change in their relative intensity and the appearance of a band at 725 -730 cm^{-1} (blue). The observed frequency change at ~730 cm^{-1} increases when going from Co(II) to Ni(II) and Mn(II) whilst the band at 711 cm^{-1} decreases. This is likely due to the strength of the interaction between the ligand and the metal and are consistent with the preferential extraction of Co(II) > Ni(II) > Mn(II) in the thymol+phen DES.

The metal saturated DES-phase were also studied by fluorescence analysis as the emission spectra is sensitive to changes in the molecular structures of the complex (Carter et al., 2014), shown in **Figure 5E**. The corresponding UV-vis spectra are available in **Figure S9**. The results show that after excitation at 425 nm corresponding to the MLCT band of the complexes, all metal complexes exhibit similar emissions in the spectral range between 480-496 nm with small but notable differences. The Mn(II) loaded DES phase exhibits emission bands at 467, 489 and at 530 nm while for Ni(II), two broad emission bands were observed centred at 480 nm and 536 nm. The Co(II) spectra is characterised by the splitting of the lower wavelength band resulting in four bands at 462, 477, 497 and 547 nm and a change in the relative intensity of the bands compared to the spectra of Ni(II) and Mn(II). Although not conclusive, spectroscopic results suggest the preferential extraction of Co(II) over Ni(II) and Mn(II) is driven by the greater strength of the Co(II)-phen interaction and small changes in the DES phase complex. However, it remains unclear as to what is the underlying reason for this divergence between the aqueous log(K_1) of complexes and the extraction profiles when phen is incorporated into a DES. Additional work probing the speciation of metals in the DES phase could provide further insight as to the differences between the extracted complexes.

Metal extraction in the thymol+phen system – extension to other systems

In this final section, the metal extraction studies in the thymol+phen system are extended to other metal families and the potential of the eutectic for metal pre-concentration and analysis is demonstrated for Fe(III) quantification. The extraction of selected metals representing different groups, namely PGMs (Pd(II)), heavy metals (Cd(II)), transition metals, alkaline earth metals (Ba(II)) and lanthanides (La(III)), was determined at [HCl] = 0.05 mol L^{-1}. The extraction efficiencies are shown in **Figure 6A** and the derived distribution coefficients are plotted against the aqueous first formation constant for each metal with phen in **Figure 6B** (Anderegg and Wanner, 1986; Hancock, 2013). The $\%EE_M$ and D_M values are available in **Table S11**. Unless otherwise specified, standard conditions were: metal concentrations of 0.02 mol L^{-1}, x_{phen} = 0.2 and an O/A ratio of 0.50 (total volume of 1.5 mL). Additionally, the water content of the DES phase following metal cation partition was measured. However, due to the low metal concentration used, no significant difference between metal systems were observed and a similar average water concentration as for the equivalent system without metal (**Table S6**) of $[H_2O]_{DES}$ = 1.49 ± 0.09 wt.% was obtained.

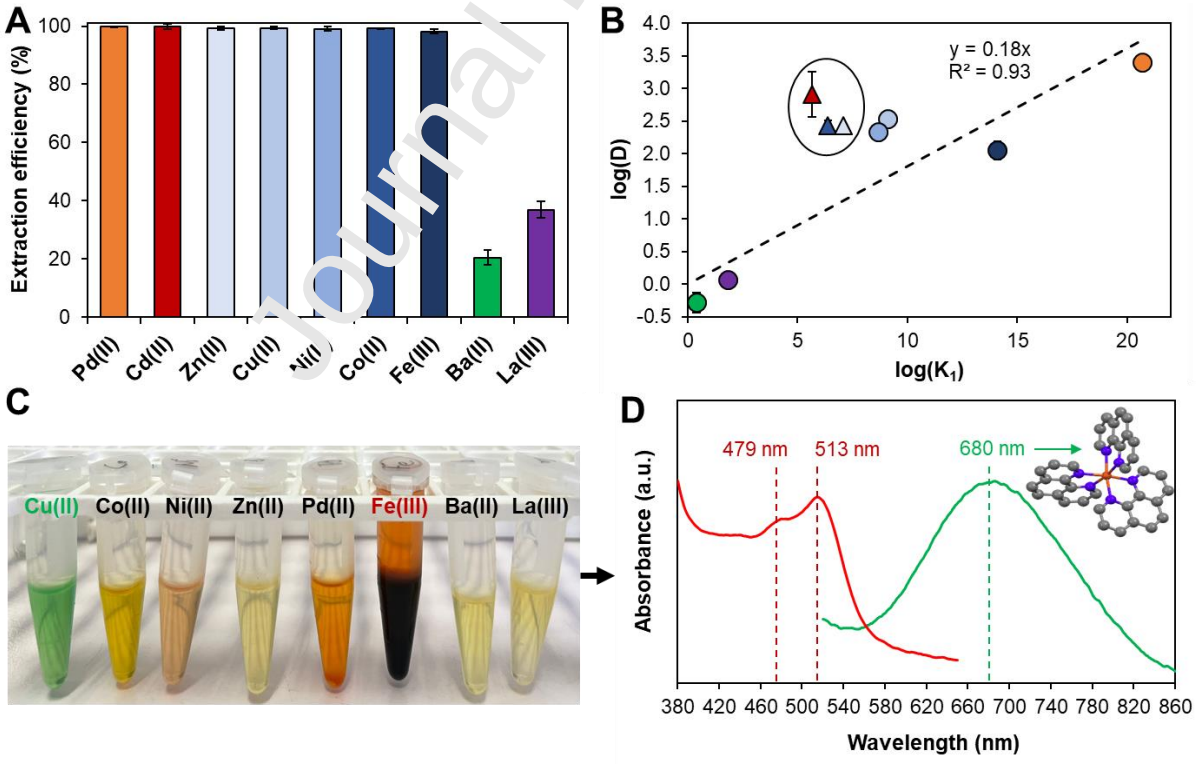

Figure 6. A) Extraction efficiencies of various metal chloride salts (mono-elemental solutions, [M] = 0.02 mol L^{-1}, pH = 1.6) in the thymol+phen eutectic (x_{phen} = 0.2; O/A =

0.50). B) Correlation of the aqueous first formation constant for each metal with phenanthroline (Anderegg and Wanner, 1986; Hancock, 2013) against the obtained distribution coefficients in the DES phase. Triangles represent points excluded from the linear regression; colour code follows that of panel (A). C) Photograph of the systems after extraction focusing on the bottom DES phase. D) UV-vis spectra of the DES phase after extraction of Fe(III) (red) and Cu(II) (green). Please refer to the online journal edition for the coloured version of this Figure.

Extraction to the DES phase is almost quantitative for metals presenting moderate to high formation constants with phen, allowing to envisage its potential application as a pre-concentration medium for analytical purposes or for transition metal/lanthanide separation with an α(Co/La) of 223. The extraction proceeds predictably with the first formation constant log(K_1) of the phen-metal complex (**Figure 6B**) although the trend between metals with close log(K_1) values is blurred due to the high phen to metal ratio as shown by the circled data points. Nevertheless, it suggests that the separation of metal pairs in the DES phase can be identified from readily available phen formation constants. The resulting loaded DES phase shown in **Figure 6C** displays the characteristic coloration of the metal-phen complexes including green for Cu(II), pink for Ni(II) and yellow for Co(II). Unexpectedly, the UV-vis spectra of Fe-loaded DES in **Figure 6D** presents the assigned peaks of the Fe(II)-phen complex (Agustina et al., 2015), signifying a reduction of Fe(III) in the DES phase most likely through the oxidation of the phenolic group of thymol. Additionally, the UV-vis spectra of the Cu-loaded DES displays a broad peak centred around 680 nm indicative of the $[Cu(phen)_3]^{2+}$ complex shown in the inset of **Figure 5D** from single crystal structure (Korpi et al., 2007; Potočňák et al., 2002), suggesting the sole presence of phen in the first coordination sphere of the extracted metals.

The reduction of Fe(III) upon extraction to the DES phase in the absence of additional reducing agent allows for the development of a facile detection technique for all aqueous Fe species, regardless of its oxidation state, whilst benefitting from the intense coloration of the Fe(II)-phen complex. To this end, 0.25 mL of DES were agitated for 1 min with various aqueous $FeCl_3$ solutions at pH = 5.5 and O/A = 0.25 (total volume 1.25 mL) and centrifuged thereafter. The DES phase was further analysed by UV-vis with the results presented in **Figure 7**. Pre-concentration of Fe in the DES phase allows for signal amplification whilst the

high phen to metal ratio ensures a high binding efficiency. The results in **Figure 7** indicate that the detection limit for Fe(II/III) ions is 12 μg L^{-1} (0.21 μmol L^{-1}) in the UV–vis mode and 58 μg L^{-1} (1.03 μmol L^{-1}) in the visual mode. The obtained detection limits are significantly lower than the recommended lower concentration of Fe^{2+} (5.36 μmol L^{-1}) in drinking water by the WHO and compare favourably to other organic Fe(II) sensors including rhodamine B (0.20 μmol L^{-1}) (Hirayama et al., 2013), *N*-aryl-*O*-acylhydroxylamine (0.50 μmol L^{-1}) (Xuan et al., 2016), arene-based fluorescent probes (8.54 μmol L^{-1}) (Kumar et al., 2015), benzimidazolyl pyridine (0.28 μmol L^{-1}) (Bhaumik et al., 2011), and phen functionalised polymers (0.05 μmol L^{-1}) (Nawaz et al., 2018). A recent study applied the hydrophobic eutectic composed of tetrabutylammonium chloride and decanoic acid with phen as chelating agent for the microextraction and determination of Ni(II) and Zn(II) by flame atomic absorption spectroscopy from various foods (Elahi et al., 2022). This suggests that if properly optimised, the system studied herein can be extended to other metals after considering the metal analysis technique, the potential interference of other ions as well as the usable pH range.

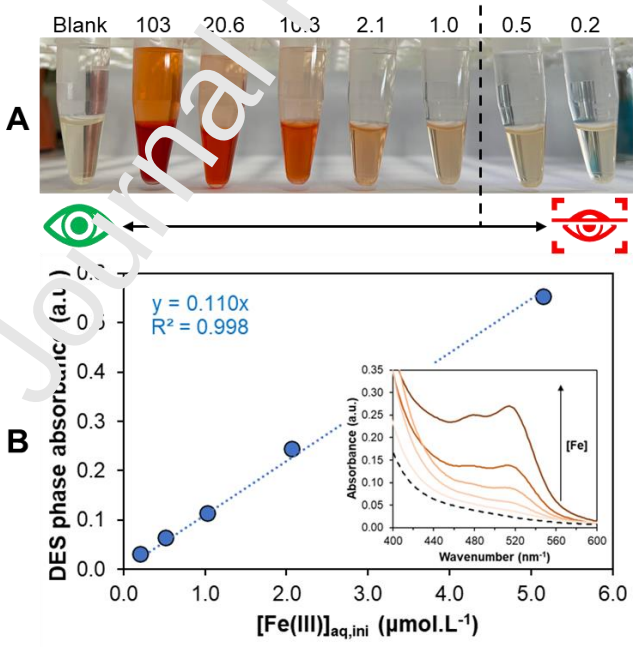

Figure 7. A) Naked eye and B) UV-vis quantification of $FeCl_3$ in the thymol+phen eutectic (pH = 5.5, O/A = 0.25, x_{phen} = 0.2). The photograph in A) was taken using an iPhone 12 and presented without modification. Please refer to the online journal edition for the coloured version of this Figure.

Conclusions

In this work, a new family of Type V DES based on the polypyridyl ligand 1,10-phenanthroline is presented and its properties thoroughly characterised with the aim of facilitating the extrapolation of the disclosed findings to other potential systems based on phen or bipyridine derivatives. The thymol+phen eutectic presents a complex SLE diagram with multiple eutectic points. The physical properties of the DES are strongly dependent on the concentration and nature of co-extracted polar solutes which is itself dependent on the acidity of aqueous phase in equilibrium. The pK_b of phen is shifted by four orders of magnitude upon inclusion as a DES component to approximately $pK_b \sim 1.0$; phen protonation has a marked impact on its aqueous phase solubility and its metal extraction capacity. The important metal chelating ability of phen are not significantly altered when included as a DES component and can be approximately predicted based on existing metal-phen formation constants. It allows for the quantitative extraction of transition and platinum group metals and their separation from lanthanides and alkaline earth ions whilst benefitting from the intrinsic properties of DES. This includes the increased process intensification (i.e. lower O/A ratio required) due to the greater solubility of phen in the DES through its liquification as well as the synergistic enhancement in hydrophobicity of the eutectic components. The new DES opens new possibilities for pre-concentration of samples, such as metals, in addition to a new class of hydrophobic extractive systems based on terpenes and complexing agents. Although the loaded DES phase possesses luminescence properties of potential interest for selected applications including metal sensing (Carter et al., 2014) or organic light-emitting diodes (Accorsi et al., 2009), additional work is required to identify a suitable regeneration protocol for its use in solvent extraction.

Declaration of Competing Interest

The authors declare that they have no known competing financial interests or personal relationships that could have appeared to influence the work reported in this paper.

Acknowledgements

This work was developed within the scope of the project CICECO-Aveiro Institute of Materials, UIDB/50011/2020, UIDP/50011/2020 & LA/P/0006/2020, financed by national funds through the FCT/MEC (PIDDAC). NMR analysis was made possible through the National NMR Network, funded within the framework of the National Program for Scientific Re-equipment, contract REDE/1517/RMN/2005 with funds from POCI 2010 (FEDER) and FCT. M.C. Hespanhol acknowledges Coordenação de Aperfeiçoamento de Pessoal de Nível Superior/Fundação para a Ciência e Tecnologia (CAPES/FCT 88881.309048/2018-01). A.P.S. Crema acknowledges CAPES for her fellowship (88887.474466/2020-00). H. Passos acknowledges FCT, I.P., under the Scientific Employment Stimulus Individual Call (CEECIND/00831/2017). N. Schaeffer acknowledges the national funds (OE), through FCT in the scope of the framework contract foreseen in the numbers 4, 5 and 6 of the article 23, of the Decree-Law 57/2016, of August 29, changed by Law 57/2017, of July 19.

References

Abraham, M.J., Murtola, T., Schulz, R., Páll, S., Smith, J.C., Hess, B., Lindah, E., 2015. Gromacs: High performance molecular simulations through multi-level parallelism from laptops to supercomputers. SoftwareX 1–2, 19–25. https://doi.org/10.1016/j.softx.2015.06.001

Abranches, D.O., Coutinho, J.A.P., 2022. Type V Deep Eutectic Solvents: Design and Applications. Curr. Opin. Green Sustain. Chem. 100612. https://doi.org/10.1016/J.COGSC.2022.100612

Abranches, D.O., Martins, M.A.R., Silva, L.P., Schaeffer, N., Pinho, S.P., Coutinho, J.A.P., 2019. Phenolic hydrogen bond donors in the formation of non-ionic deep eutectic solvents: The quest for type v des. Chem. Commun. 55, 10253–10256. https://doi.org/10.1039/c9cc04846d

Abranches, D.O., Silva, L.P., Martins, M.A.R., Coutinho, J.A.P., 2021. Differences on the impact of water on the deep eutectic solvents betaine/urea and choline/urea. J. Chem. Phys. 155, 034501. https://doi.org/10.1063/5.0052303

Accorsi, G., Listorti, A., Yoosaf, K., Armaroli, N., 2009. 1,10-Phenanthrolines: versatile building blocks for luminescent molecules, materials and metal complexes. Chem. Soc. Rev. 38, 1690–1700. https://doi.org/10.1039/B806408N

Agustina, E., Goak, J., Lee, S., Seo, Y., Park, J.Y., Lee, N., 2015. Simple and Precise Quantification of Iron Catalyst Content in Carbon Nanotubes Using UV/Visible Spectroscopy. ChemistryOpen 4, 613–619. https://doi.org/10.1002/OPEN.201500096

Anderegg, G., 1963a. Pyridinderivate als Komplexbildner V. Die Metallkomplexe von 1,10-Phenanthrolin und α, α′-Dipyridyl. Helv. Chim. Acta 46, 2397–2410. https://doi.org/10.1002/HLCA.19630460657

Anderegg, G., 1963b. Pyridinderivate als Komplexbildner VI. Reaktionsenthalpie und -entropie bei der Bildung der Metallkomplexe von 1,10-Phenanthrolin und α,α′-Dipyridyl. Helv. Chim. Acta 46, 2813–2822. https://doi.org/10.1002/HLCA.19630460740

Anderegg, G., Wanner, H., 1986. Pyridine derivatives as complexing agents. XIII. The stability of the palladium(II) complexes with pyridine, 2,2′-bipyridyl, and 1,10-phenanthroline. Inorganica

Chim. Acta 113, 101–108. https://doi.org/10.1016/S0020-1693(00)82229-X

Armaroli, N., De Cola, L., Balzani, V., Sauvage, J.P., Dietrich-Buchecker, C.O., Kern, J.M., 1992. Absorption and luminescence properties of 1, 10-phenanthroline, 2, 9-diphenyl-1, 10-phenanthroline, 2,9-dianisyl-1, 10-phenanthroline and their protonated forms in dichloromethane solution. J. Chem. Soc. Faraday Trans. 88, 553–556. https://doi.org/10.1039/FT9928800553

Becke, A.D., 1988. Density-Functional Exchange-Energy Approximation with Correct Asymptotic Behavior. Phys. Rev. A 38, 3098–3100. https://doi.org/10.1103/PhysRevA.38.3098

Bencini, A., Lippolis, V., 2010. 1,10-Phenanthroline: A versatile building block for the construction of ligands for various purposes. Coord. Chem. Rev. https://doi.org/10.1016/j.ccr.2010.04.008

Berendsen, H.J.C., Grigera, J.R., Straatsma, T.P., 1987. The missing term in effective pair potentials. J. Phys. Chem. 91, 6269–6271. https://doi.org/10.1021/j100308a038

Bhaumik, C., Das, S., Maity, D., Baitalik, S., 2011. A terpyridyl imidazole (tpy-HImzPh3) based bifunctional receptor for multichannel detection of Fe2+ and F− ions. Dalt. Trans. 40, 11795–11808. https://doi.org/10.1039/C1DT10965K

BIOVIA COSMOtherm, Release 2021; Dassault Systèmes. http://www.3ds.com, n.d.

Bonthuis, D.J., Mamatkulov, S.I., Netz, R.R., 2016. Optimization of classical nonpolarizable force fields for OH- and H3O+. J. Chem. Phys. 144, 104503. https://doi.org/10.1063/1.4942771

Bourgeois, D., El Maangar, A., Dourdain, S., 2020. Importance of weak interactions in the formulation of organic phases for efficient liquid/liquid extraction of metals. Curr. Opin. Colloid Interface Sci. 46, 36–51. https://doi.org/10.1016/J.COCIS.2020.03.004

Bramley, A., 1916. XXXVII.—The study of binary mixtures. Part III. Freezing-point curves. J. Chem. Soc. Trans. 109, 469–496. https://doi.org/10.1039/CT9160900469

Brehm, M., Kirchner, B., 2011. TRAVIS - A free analyzer and visualizer for monte carlo and molecular dynamics trajectories. J. Chem. Inf. Model. 51, 2007–2023. https://doi.org/10.1021/ci200217w

Brehm, M., Weber, H., Thomas, M., Hollóczki, O., Kirchner, B., 2015a. Domain Analysis in Nanostructured Liquids: A Post-Molecular Dynamics Study at the Example of Ionic Liquids. ChemPhysChem 16, 3271–3277. https://doi.org/10.1002/cphc.201500471

Brehm, M., Weber, H., Thomas, M., Hollóczki, O., Kirchner, B., 2015b. Domain Analysis in Nanostructured Liquids: A Post-Molecular Dynamics Study at the Example of Ionic Liquids. ChemPhysChem 16, 3271–3277. https://doi.org/10.1002/cphc.201500471

Breneman, C.M., Wiberg, K.B., 1990. Determining Atom-Centered Monopoles from Molecular Electrostatic Potentials. The Need for High Sampling Density in formamide Conformational Analysis. J. Comput. Chem. 11, 361–373. https://doi.org/10.1002/jcc.540110311

Burchett, S., Meloan, C.E., 1972. Infrared studies of water bound to some extracted phenanthroline and phenanthroline chelates. J. Inorg. Nucl. Chem. 34, 1207–1213. https://doi.org/10.1016/0022-1902(72)80321-X

Burgess, J., Haines, R.I., 2002. Solubilities of 1,10-phenanthroline and substituted derivatives in water and in aqueous methanol. J. Chem. Eng. Data 23, 196–197. https://doi.org/10.1021/JE60078A009

Byrne, E.L., O'Donnell, R., Gilmore, M., Artioli, N., Holbrey, J.D., Swadźba-Kwaśny, M., 2020. Hydrophobic functional liquids based on trioctylphosphine oxide (TOPO) and carboxylic acids. Phys. Chem. Chem. Phys. 22, 24744–24763. https://doi.org/10.1039/d0cp02605k

Carolan, A.N., Mroz, A.E., El Ojaimi, M., Vanderveer, D.G., Thummel, R.P., Hancock, R.D., 2012.

Metal-ion-complexing properties of 2-(pyrid-2′-yl)-1,10- phenanthroline, a more preorganized analogue of terpyridyl. A crystallographic, fluorescence, and thermodynamic study. Inorg. Chem. 51, 3007–3015. https://doi.org/10.1021/IC202337V

Carter, K.P., Young, A.M., Palmer, A.E., 2014. Fluorescent Sensors for Measuring Metal Ions in Living Systems. Chem. Rev. 114, 4564–4601. https://doi.org/10.1021/CR400546E

Clark, A.E., 2019. Amphiphile-Based Complex Fluids: The Self-Assembly Ensemble as Protagonist. ACS Cent. Sci. 5, 10–12. https://doi.org/10.1021/acscentsci.8b00927

Coutinho, J.A.P., Andersen, S.I., Stenby, E.H., 1995. Evaluation of activity coefficient models in prediction of alkane solid-liquid equilibria. Fluid Phase Equilib. 103, 23–39. https://doi.org/10.1016/0378-3812(94)02600-6

Darden, T., York, D., Pedersen, L., 1993. Particle mesh Ewald: An N·log(N) method for Ewald sums in large systems. J. Chem. Phys. 98, 10089–10092. https://doi.org/10.1063/1.464397

Dean, P.M., Turanjanin, J., Yoshizawa-Fujita, M., MacFarlane, D.R., Scott, J.L., 2009. Exploring an anti-crystal engineering approach to the preparation of pharmaceutically active ionic liquids. Cryst. Growth Des. 9, 1137–1145. https://doi.org/10.1021/CG8009496/SUPPL_FILE/CG8009496_SI_001.PDF

Eckert, F., Klamt, A., 2002. Fast Solvent Screening via Quantum Chemistry: COSMO-RS Approach. AIChE J. 48, 369–385. https://doi.org/10.1002/aic.690480220

Edgecomb, J., Tereshatov, E., Zante, G., Boltoeva, M., Folden III, C.M., 2020. Hydrophobic amine-based binary mixtures of active pharmaceutical and food grade ingredients: characterization and application in indium extraction from aqueous hydrochloric acid media. Green Chem. https://doi.org/10.1039/d0gc02452j

Elahi, F., Arain, M.B., Ali Khan, W., Ul Haq, H., Khan, A., Jan, F., Castro-Muñoz, R., Boczkaj, G., 2022. Ultrasound-assisted deep eutectic solvent-based liquid–liquid microextraction for simultaneous determination of Ni (II) and Zn (II) in food samples. Food Chem. 393, 133384. https://doi.org/10.1016/J.FOODCHEM.2022.133384

Evans, D.J., Holian, B.L., 1985. The Nose-Hoover thermostat. J. Chem. Phys. 83, 4069–4074. https://doi.org/10.1063/1.449071

Frisch, M.J., et al., n.d. Gaussian 09 (revision D.01); Gaussian, Inc.: Wallingford, CT, USA, 2009.

Gilli, P., Pretto, L., Bertolasi, V., Gilli, G., 2009. Predicting Hydrogen-Bond strengths from Acid-Base molecular properties. the pKa slide rule: Toward the solution of a Long-Lasting problem. Acc. Chem. Res. 42, 33–44. https://doi.org/10.1021/ar800001k

Gilmore, M., McCourt, É.N., Connolly, F., Nockemann, P., Swadźba-Kwaśny, M., Holbrey, J.D., 2018. Hydrophobic Deep Eutectic Solvents Incorporating Trioctylphosphine Oxide: Advanced Liquid Extractants. ACS Sustain. Chem. Eng. 6, 17323–17332. https://doi.org/10.1021/acssuschemeng.8b04843

Hammond, O.S., Bowron, D.T., Edler, K.J., 2017. The Effect of Water upon Deep Eutectic Solvent Nanostructure: An Unusual Transition from Ionic Mixture to Aqueous Solution. Angew. Chemie - Int. Ed. 56, 9782–9785. https://doi.org/10.1002/anie.201702486

Hanada, T., Goto, M., 2021. Synergistic Deep Eutectic Solvents for Lithium Extraction. ACS Sustain. Chem. Eng. 9, 2152–2160. https://doi.org/10.1021/acssuschemeng.0c07606

Hancock, R.D., 2013. The pyridyl group in ligand design for selective metal ion complexation and sensing. Chem. Soc. Rev. 42, 1500–1524. https://doi.org/10.1039/C2CS35224A

Herrington, R., 2021. Mining our green future. Nat. Rev. Mater. 2021 66 6, 456–458. https://doi.org/10.1038/s41578-021-00325-9

Hess, B., Bekker, H., Berendsen, H.J.C., Fraaije, J.G.E.M., 1997. LINCS: A Linear Constraint Solver for molecular simulations. J. Comput. Chem. 18, 1463–1472. https://doi.org/10.1002/(SICI)1096-987X(199709)18:12<1463::AID-JCC4>3.0.CO;2-H

Hirayama, T., Okuda, K., Nagasawa, H., 2013. A highly selective turn-on fluorescent probe for iron(II) to visualize labile iron in living cells. Chem. Sci. 4, 1250–1256. https://doi.org/10.1039/C2SC21649C

Hockney, R.W., Goel, S.P., Eastwood, J.W., 1974. Quiet high-resolution computer models of a plasma. J. Comput. Phys. 14, 148–158. https://doi.org/10.1016/0021-9991(74)90010-2

Honeywell Research Chemicals, n.d. 1,10-Phenanthroline hydrochloride monohydrate [WWW Document]. URL https://lab.honeywell.com/shop/1-10-phenanthroline-hydrochloride-monohydrate-31043 (accessed 3.15.22).

Humphrey, W., Dalke, A., Schulten, K., 1996. VMD: Visual molecular dynamics. J. Mol. Graph. 14, 33–38. https://doi.org/10.1016/0263-7855(96)00018-5

Isabel Cabaço, M., Besnard, M., Morgado, P., Filipe, E.J.M., Coutinho, J.A.P., Danten, Y., 2021. Gaseous hetero dimers of perfluoro tert-butyl alcohol with hydrogenated alcohols by infrared spectroscopy and quantum DFT calculations. Chem. Phys. 544, 111110. https://doi.org/10.1016/J.CHEMPHYS.2021.111110

Klamt, A., 1995. Conductor-like Screening Model for Real Solvents: A New Approach to the Quantitative Calculation of Solvation Phenomena. J. Phys. Chem. 99, 2224–2235. https://doi.org/10.1021/j100007a062

Klamt, A., Jonas, V., Bürger, T., Lohrenz, J.C.W., 1998. Refinement and Parametrization of COSMO-RS. J. Phys. Chem. A 102, 5074–5085. https://doi.org/10.1021/jp980017s

Korpi, H., Figiel, P.J., Lankinen, E., Ryan, P., Leskelä, M., Repo, T., 2007. On In Situ Prepared Cu–Phenanthroline Complexes in Aqueous Alkaline Solutions and Their Use in the Catalytic Oxidation of Veratryl Alcohol. Eur. J. Inorg. Chem. 2007, 2465–2471. https://doi.org/10.1002/EJIC.200600908

Kumar, P., Kumar, V., Gupta, R., 2015. Arene-based fluorescent probes for the selective detection of iron. RSC Adv. 5, 97874–97882. https://doi.org/10.1039/C5RA20760F

Lee, C., Yang, W., Parr, R.G., 1988. Development of the Colle-Salvetti Correlation-Energy Formula Into a Functional of the Electron Density. Phys. Rev. B 37, 785–789. https://doi.org/10.1103/PhysRevB.37.785

Lewis, F.W., Harwood, L.M., Hudson, M.J., Drew, M.G.B., Desreux, J.F., Vidick, G., Bouslimani, N., Modolo, G., Wilden, A., Sypula, M., Vu, T.-H., Simonin, J.-P., 2011. Highly Efficient Separation of Actinides from Lanthanides by a Phenanthroline-Derived Bis-triazine Ligand. J. Am. Chem. Soc 133, 18. https://doi.org/10.1021/ja203378m

Martins, M.A.R., Crespo, E.A., Pontes, P.V.A., Silva, L.P., Bülow, M., Maximo, G.J., Batista, E.A.C., Held, C., Pinho, S.P., Coutinho, J.A.P., 2018. Tunable Hydrophobic Eutectic Solvents Based on Terpenes and Monocarboxylic Acids. ACS Sustain. Chem. Eng. 6, 8836–8846. https://doi.org/10.1021/acssuschemeng.8b01203

Meijler, M.M., Zelenko, O., Sigman, D.S., 1997. Chemical Mechanism of DNA Scission by (1,10-Phenanthroline)copper. Carbonyl Oxygen of 5-Methylenefuranone Is Derived from Water. J. Am. Chem. Soc. 119, 1135–1136. https://doi.org/10.1021/JA962409N

Motokawa, R., Kobayashi, T., Endo, H., Mu, J., Williams, C.D., Masters, A.J., Antonio, M.R., Heller, W.T., Nagao, M., 2019. A Telescoping View of Solute Architectures in a Complex Fluid System. ACS Cent. Sci. 5, 85–96. https://doi.org/10.1021/acscentsci.8b00669

Muniz-Miranda, M., Pergolese, B., Bigotto, A., 2010. SERS and DFT investigation on the adsorption of 1,10-phenanthroline on transition metal surfaces. Phys. Chem. Chem. Phys. 12, 1145–1151. https://doi.org/10.1039/B913014D

Nawaz, H., Tian, W., Zhang, Jinming, Jia, R., Chen, Z., Zhang, Jun, 2018. Cellulose-Based Sensor Containing Phenanthroline for the Highly Selective and Rapid Detection of Fe2+ Ions with Naked Eye and Fluorescent Dual Modes. ACS Appl. Mater. Interfaces 10, 2114–2121. https://doi.org/10.1021/ACSAMI.7B17342

Ni, S., Su, J., Zhang, H., Zeng, Z., Zhi, H., Sun, X., 2021. A cleaner strategy for comprehensive recovery of waste SmCo magnets based on deep eutectic solvents. Chem. Eng. J. 412, 128602. https://doi.org/10.1016/j.cej.2021.128602

Parrinello, M., Rahman, A., 1981. Polymorphic transitions in single crystals: A new molecular dynamics method. J. Appl. Phys. 52, 7182–7190. https://doi.org/10.1063/1.328693

Peloquin, A.J., McCollum, J.M., McMillen, C.D., Pennington, W.T., 2021. Halogen Bonding in Dithiane/Iodofluorobenzene Mixtures: A New Class of Hydrophobic Deep Eutectic Solvents. Angew. Chemie Int. Ed. 60, 22983–22989. https://doi.org/10.1002/ANIE.202110520

Percevault, L., Jani, A., Sohier, T., Noirez, L., Paquin, L., Gauffre, F., Morineau, D., 2020. Do Deep Eutectic Solvents Form Uniform Mixtures Beyond Molecular Microheterogeneities? J. Phys. Chem. B acs.jpcb.0c06317. https://doi.org/10.1021/acs.jpcb.0c06317

Potočňák, I., Pohlová, M., Wagner, C., Jäger, L., 2002. Tris(1,10-phenanthroline)copper(II) tricyanomethanide. Acta Crystallogr. Sect. E Struct. Reports Online 58, m595–m596. https://doi.org/10.1107/S1600536802017610/BT6103ISUP2.HKL

Prausnitz, J. M.; Lichtenthaler, R. N.; Azevedo, E.G. de. ., 1999. Molecular Thermodynamics of Fluid-Phase Equilibria, 3rd ed. ed. Prentice Hall, Upper Saddle River, NJ.

Rajput, M.K., Konwar, M., Sarma, D., 2021. Hydrophobic natural deep eutectic solvent THY-DA as sole extracting agent for arsenic (III) removal from aqueous solutions. Environ. Technol. Innov. 24, 102017. https://doi.org/10.1016/J.ETI.2021.102017

Sammes, P.G., Yahioglu, G., 1994. 1,10-Phenanthroline: a versatile ligand. Chem. Soc. Rev. 23, 327–334. https://doi.org/10.1039/CS9942300327

Sarmini, K., Kenndler, E., 1999. Ionization constants of weak acids and bases in organic solvents. J. Biochem. Biophys. Methods 38, 123–137. https://doi.org/10.1016/S0165-022X(98)00033-5

Schaeffer, N., Abranches, D.O., Silva, L.P., Martins, M.A.R., Carvalho, P.J., Russina, O., Triolo, A., Paccou, L., Guinet, Y., Hedoux, A., Coutinho, J.A.P., 2021. Non-Ideality in Thymol + Menthol Type V Deep Eutectic Solvents. ACS Sustain. Chem. Eng. https://doi.org/10.1021/acssuschemeng.0c07874

Schaeffer, N., Conceição, J.H.F., Martins, M.A.R., Neves, M.C., Pérez-Sánchez, G., Gomes, J.R.B., Papaiconomou, N., Coutinho, J.A.P., 2020. Non-ionic hydrophobic eutectics-versatile solvents for tailored metal separation and valorisation. Green Chem. 22, 2810–2820. https://doi.org/10.1039/d0gc00793e

Schaeffer, N., Martins, M.A.R., Neves, C.M.S.S., Pinho, S.P., Coutinho, J.A.P., 2018. Sustainable hydrophobic terpene-based eutectic solvents for the extraction and separation of metals. Chem. Commun. 54. https://doi.org/10.1039/c8cc04152k

SigmaAldrich, 2022. Chemical SDS [WWW Document]. URL https://www.sigmaaldrich.com

Smith, E.L., Abbott, A.P., Ryder, K.S., 2014. Deep Eutectic Solvents (DESs) and Their Applications. Chem. Rev. https://doi.org/10.1021/cr300162p

Thornton, D.A., Watkins, G.M., 1991. A full vibrational assignment (4000-50 cm−1) of 1, 10-

phenanthroline and its perdeuterated analogue. Spectrochim. Acta Part A Mol. Spectrosc. 47, 1085–1096. https://doi.org/10.1016/0584-8539(91)80039-L

Tucker, L.E., Littman, G.C., Uritis, S., Nugent, J.W., Thummel, R.P., Reibenspies, J.H., Jones, S.B., Lee, H.S., Hancock, R.D., 2020. Fluorescence and Metal-Binding Properties of the Highly Preorganized Tetradentate Ligand 2,2′-Bi-1,10-phenanthroline and Its Remarkable Affinity for Cadmium(II). Inorg. Chem. 59, 13117–13127. https://doi.org/10.1021/ACS.INORGCHEM.0C00361

TURBOMOLE V7.1 2016, a development of University of Karlsruhe and Forschungszentrum Karlsruhe GmbH, 1989-2007, TURBOMOLE GmbH, since 2007; available from http://www.turbomole.com., n.d.

Vargas, S.J.R., Pérez-Sánchez, G., Schaeffer, N., Coutinho, J.A.P., 2021. Solvent extraction in extended hydrogen bonded fluids – separation of Pt(IV) from Pd(II) using TOPO-based type V DES. Green Chem. 23, 4540–4550. https://doi.org/10.1039/D1GC00829C

Xu, L., Zhang, A., Lu, Y., Yang, H., Liu, Z., 2016. A phenanthroline-derived ligand and its complexation with Pd(II): from ligand design, synthesis and Pd(II) complexes structures to its application. RSC Adv. 6, 99859–99866. https://doi.org/10.1039/C6RA20484H

Xuan, W., Pan, R., Wei, Y., Cao, Y., Li, H., Liang, F. Sen, Liu, K.J., Wang, W., 2016. Reaction-Based "Off-On" Fluorescent Probe Enabling Detection of Endogenous Labile Fe2+ and Imaging of Zn2+-induced Fe2+ Flux in Living Cells and Elevated Fe2+ in Ischemic Stroke. Bioconjug. Chem. 27, 302–308. https://doi.org/10.1021/ACS.BIOCONJCHEM.5B00259

Author Statement

Anna P.S. Crema: Investigation, Visualization, Writing – original draft. **Nicolas Schaeffer**: Investigation, Conceptualization, Visualization, Supervision, Writing – original draft. **Henrique Bastos**: Investigation. **Liliana P. Silva**: Investigation. **Dinis O. Abranches:** Investigation, Conceptualization. **Helena Passos:** Investigation, Visualization, Supervision. **Maria C. Hespanhol:** Funding acquisition, Conceptualization, Supervision. **João A.P. Coutinho:** Resources, Funding acquisition, Conceptualization, Supervision.

All authors participated in the reviewing and editing of this work.

Declaration of interests

☒The authors declare that they have no known competing financial interests or personal relationships that could have appeared to influence the work reported in this paper.

☐The authors declare the following financial interests/personal relationships which may be considered as potential competing interests:

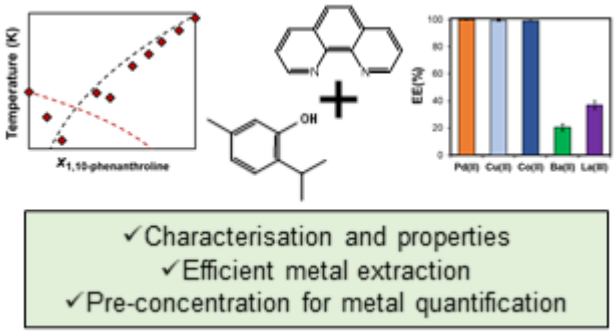

✓Characterisation and properties
✓Efficient metal extraction
✓Pre-concentration for metal quantification

Highlights

- Characterisation of a new family of hydrophobic eutectic solvents based on 1,10-phenanthroline and natural phenolic compounds.
- Excellent metal extraction capabilities for transition metals.
- Protonation of 1,10-phenanthroline under acidic conditions reduces metal partition and alters the properties of the eutectic solvent.
- Pre-concentration and detection of Fe(II/III) to μg L^{-1} levels was achieved in the thymol+phenanthroline system.